Biomass Pyrolysis and Gasification of Varying Particle Sizes in a Fluidized-Bed Reactor

Katherine R. Gaston,* Mark W. Jarvis, Perrine Pepiot, Kristin M. Smith, William J. Frederick, Jr., and Mark R. Nimlos

National Bioenergy Center, National Renewable Energy Laboratory, 1617 Cole Boulevard, Golden, Colorado 80401, United States

S *Supporting Information*

ABSTRACT: A new 4 in. (102 mm) diameter fluidized-bed reactor has been built and used to study the effect of biomass particle size on the yield of light gas and tar compounds during gasification. Batch experiments were conducted with white oak milled into four sphere sizes with diameters of 6, 13, 18, and 25 mm, at reactor bed temperatures of 500, 600, 700, 800, and 900 °C. As expected, the yields of light gas increase with temperature but then reach a plateau above 800 °C. As the particle size increases, a decrease in the formation of light gases, accompanied by an increase in the formation of char, is observed. For larger particle sizes, the commonly used power law dependence of particle devolatilization time with sphere diameter holds true and the transition from heat- and mass-transport control to kinetic control as particle diameter decreases is illustrated. Measurements of the organic compounds present in the syngas are performed using a molecular beam mass spectrometer (MBMS). These measurements indicate that, as the size of the spheres increases, the formation of tars and polycyclic aromatic hydrocarbons (PAHs) increases. These observations further emphasize the important role of heat- and mass-transport restrictions for larger particles in the evolution of products during gasification and its potential implications on gasification process economics.

INTRODUCTION

Transportation fuels produced from biomass have received a great deal of interest lately because of the potential advantages of this renewable energy source in terms of fossil fuel displacement and greenhouse gas emissions. There are a variety of conversion technologies being considered for the production of fuels, including biological disassembly and fermentation, pyrolysis, and gasification. One of the major challenges in the production of biofuels from gasification and synthesis is the formation of high-molecular-weight species called tars during the gasification process. Tars detract from synthesis gas (syngas) yields and have to be removed prior to the fuel synthesis step to prevent deactivation of the catalysts and fouling of process equipment. Tars encompass a wide variety of compounds, which can be grouped into classes depending upon their chemical characteristics,[1−3] from heterocyclic compounds, such as phenol or cresols, to polycyclic aromatic hydrocarbon (PAH) species. The latter ones are highly refractory and condense at relatively high temperatures. As a result, their removal from the syngas requires expensive treatments, such as catalytic steam reforming, which has a significant impact on the process economics.[4]

A more cost-effective approach therefore would be to improve the gasification process to mitigate the formation of these species prior the gas-cleaning stage. Such primary measures have been the topic of a large volume of work, especially for fluidized beds,[2,5−10] and the impact of bed and freeboard temperature, gasifying agent, superficial velocity, gas residence time, bed additives, such as dolomite or olivine, biomass injection location, secondary air injection, and equivalence ratio (in the case of air-blown gasification) on the syngas heating value and char, tar, and gas yields have been investigated extensively. In particular, it was

shown that operating conditions, especially temperature, can dramatically alter the tar composition, with substituted and oxygen-containing compounds being replaced by non-substituted aromatic species as the temperature increases.[1,11,12] It must be noted though that most of those studies used air as the gasifying medium, which significantly increases the reactivity of the chemical mixture. Much less studied is the impact of particle size on the amount and composition of tar formed during gasification,[13,14] even though such information is of prime importance for reactor design. Indeed, most preliminary design and optimization research is performed at the laboratory scale, using either fine powder or millimeter-sized particles for ease of processing and residence time limitations. Because any preprocessing of biomass adds to the cost of biofuel production by requiring additional capital equipment, labor, and processing time, commercial-scale units will instead operate with much larger biomass particles. Failure to account for the differences in the nature and amount of the tar produced from larger particles introduces uncertainties in the scale-up process and will result in lower-than-expected efficiency of primary tar mitigation measures and ill-designed downstream cleanup equipment.

The role of biomass structure and heat and mass transport inside biomass particles in the conversion process is widely recognized. Even for particle sizes usually associated with kinetic control and negligible heat- and mass-transfer limitations, the biomass structure changes dramatically over the course of the devolatilization process (i.e., process whereby volatiles in
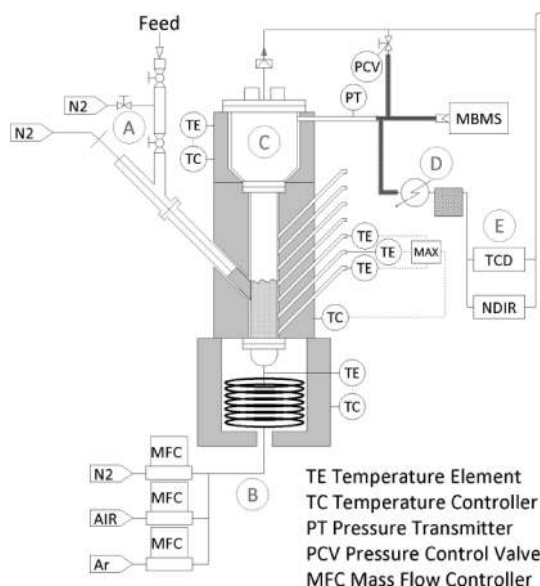
Figure 1. Experimental apparatus is shown: (A) block-and-bleed feed system, (B) fluidizing gas into preheater, (C) 4FBR reactor with freeboard and flanges at bottom, midpoint, and top, (D) gas cleanup coldfinger heat exchanger and coalescing filter, and (E) analytical equipment measuring permanent gases.

biomass enter the gas phase) and may affect chemistry significantly through product entrapment inside swelling cell walls.[11,15] At larger scales, most experimental and modeling work has focused on reliably quantifying biomass devolatilization time for practical particle sizes, because of the importance of this parameter in reactor design. Empirical correlations have been developed that typically relate devolatilization time, temperature, and particle diameters using a power law. Such expressions can be modified to account for temperature variation[13] or particle shape.[16] They involve several free parameters that have to be fitted to existing experimental data and, therefore, can vary significantly depending upon the feedstock and operating conditions.[17,18]

A more fundamental approach involves directly solving the heat- and mass-transport equations inside the particle, and a comprehensive review of such models can be found in the very good review by Di Blasi.[19] While they may be able to accurately reproduce experimental devolatilization times for a wide range of conditions[19−21] and particle shape and size,[22] these models usually carry a large number of assumptions and ad hoc parameters. Global kinetic schemes describing the conversion of biomass to char, gas, and tar can be coupled to the heat- and mass-transport equations to provide the ratio of those classes of products when they exit the particles,[19,23,24] but few studies investigate the link between intraparticle processes and actual tar amounts at the scale of the reactor. Gasification experiments at relatively low temperatures (up to 800 °C) by Herguido et al.[14] suggest larger gas yield and lower tar yield for small particles, but the use of different feedstocks precludes any definite conclusion. Systematic studies, for example by Jand and Foscollo,[25] Rapagnà et al.,[13] or Hernandez et al.,[26] demonstrate experimentally that a reduction in particle size leads to a significant improvement in the gasification parameters, especially in terms of tar amount and producer gas efficiency. Those studies did not characterize the changes in tar composition as

the particle size was varied and, thus, did not provide a complete picture of the particle size issue.

In this study, we have investigated the gasification of oak spheres of different sizes in a 4 in. fluidized-bed reactor (4FBR) using an inert gasifying agent. Products have been characterized using a molecular beam mass spectrometer (MBMS), while light gases have been measured using nondispersive infrared detectors (NDIRs). Light gases, char, and tar evolution as function of the bed temperature and particle size have been compared to literature data. A thorough analysis of the MBMS spectra provides more detailed information on the nature of the tar produced and the role played by particle size and temperature. Emphasis is set on PAH species, because those are the most problematic because of their propensity to condense at high temperature and their slow thermal cracking rates. In agreement with previous work,[11] the experimental results suggest that intraparticle chemical processes may control to a significant extent the composition of the tar at the outlet of the gasification reactor.

■ EXPERIMENTAL SECTION

To study the effect of particle size on tar formation and composition, batch experiments were conducted using a new, 4 in. diameter fluidized-bed gasifier. A schematic diagram of the reactor is shown in Figure 1. The reactor has a side arm for injecting batches of biomass and is fully instrumented for analysis of the light gases and tars, as shown below.

4FBR Apparatus. The 4FBR was designed to investigate gasification and pyrolysis on the bench scale to allow for rapid scanning of experimental conditions and enable a detailed understanding of reactor conditions and their impact on products. The reactor is integrated into a portable cart containing all required equipment for its operation: piping, heaters and insulation, gas cleanup equipment, instrumentation, control system equipment, and a power distribution panel. Figure 1 shows a schematic diagram of the reactor system, and Table 1 gives a detailed mechanical description. The system is designed to operate at internal temperatures up to 950 °C and pressures up to 80 kPa. All heated portions of the reactor are made of Incoloy or Inconel to withstand the high temperatures and possible exposure to sulfur-containing gases; likewise, all connections on the reactor are either flanged or welded. Incoloy/ceramic, spiral-wound gaskets fit between each flange, with two gaskets on either side of the distributor plate in the bottom flange.

The batch-wise feed system on the gasifier (Figure 1A) consists of a three-valve, nitrogen block-and-bleed system and a downward-angled feed tube with a nitrogen-purged plunger. The plunger was designed to remain at the base of the feed tube during gasification and was machined to complete the wall of the reactor. This prevents olivine and gas from escaping through the feed tube and minimizes disruptions from the feed tube on the fluid mechanics of the fluidized bed. Olivine can also be loaded through this port.

A supervisory control and data acquisition system (SCADA) integrates the control for the 4FBR into one Opto22 controller with a human−machine interface, which is also configured to collect data at intervals down to 0.5 s. This system monitors all temperatures, pressures, flows, and analytical instruments; it controls all heaters and mass flow controller set points. It also provides alarms and shutdowns in the case of high temperatures or pressures and mass flow controller errors.

Gas Analysis. An MBMS was used to analyze the tar species formed, while other instruments were used to analyze the key light gases. Most of the exhaust gas flowed past the inlet orifice of the MBMS, where roughly 3 sL min^{-1} of the gas was drawn into the vacuum chamber of the instrument. In the MBMS, the gas undergoes an adiabatic expansion, is

Table 1. Detailed Description of the 4FBR Reactor and Heaters, Given in Order from the Top of the Reactor down

component	description	material	purpose/function
top flange with viewports	standard 6 in. flange with two, N_2-purged quartz sight glasses and one $^3/_4$ in. sample port	Incoloy	allows for imaging reactor contents
freeboard	6 in. (154 mm), schedule 40 pipe, 30 cm long	Incoloy	reduces linear velocity of gas at the outlet to retain bed material
freeboard heater	5400 W, 17 in. outer diameter, 15 in. height	8 in. thick formed ceramic	heats freeboard to 950 °C
main exhaust	$^1/_2$ in. pipe welded perpendicularly to the wall of the freeboard with three small baffles	Incoloy	all gas exits here; baffles deflect olivine to reduce the amount that exits the reactor
reducing cone	4 to 6 in., schedule 40 cone	Incoloy	transition from the main body to the freeboard
main body	4 in. (102 mm), schedule 40 pipe, 61 cm long	Incoloy	contains hot bubbling bed where feed is gasified
main body heater	9000 W, 17 in. outer diameter, 25 in. height	8 in. thick formed ceramic	heats the main body of the reactor with fluidizing to 950 °C
feed port	2 in., schedule 40 pipe at a 45° angle to the main body, 20 cm above the distributor plate	Incoloy	used to feed biomass into the top of the bubbling bed
sample ports	seven at 45° to the reactor body; evenly spaced along the length of the reactor	Incoloy	for these experiments, top four were not used, bottom three contained thermocouples to measure the bed temperature
distributor plate	dual layer with 18 evenly spaced, 2 mm diameter holes per plate; rotational offset of 60° between the two plates	Incoloy	allows gas to uniformly fluidize bed material, while preventing material from falling into bell cap
bell cap	4 in., schedule 40 bell cap	Incoloy	fluidizing gas expands into bell cap before going through the distributor plate
coiled preheater	7.9 m of $^1/_4$ in. tubing followed by 24 m of $^3/_8$ in. tubing	$^1/_4$ in. is 316SS; $^3/_8$ in. is Inconel	preheats fluidizing gas to the reactor temperature
preheater heater	3000 W, 22 in. outer diameter, 22 in. height	8 in. thick formed ceramic	designed to heat 1.5 kg h^{-1} of nitrogen gas to 900 °C at the inlet of the reactor

skimmed into a molecular beam, and then sent to the ionization region of an on-axis triple−quadrupole mass spectrometer. The expansion effectively freezes the chemistry occurring in the reactor and improves the sensitivity of the instrument. This instrument has the advantage of universal detection and can measure signals for a wide variety of molecular species from the pyrolysis and gasification of biomass. In particular, it is well-suited for measuring and differentiating the large molecules that make up what is referred to as tars.[11,27−32] Mass spectra containing ions with mass/charge ratios (m/z) between 10 and 450 were measured and recorded once per second. Except for fragment ions, this ratio can be taken as the molecular weight of the measured species. Excess gas not drawn into the MBMS was released into the local exhaust ventilation or directed to the light gas analyzers. The line to the MBMS was kept above 500 °C to prevent vapors from condensing in the lines before reaching the MBMS inlet.

For the MBMS data analysis, relative quantities of different tar species were calculated by integrating the measured mass spectral intensity over the duration of the gas pulse obtained for each batch experiment. The spectra were normalized with each other by the intensity of the argon signal, m/z 40. To estimate and compare the total tar yields, the total ion signal for even-numbered masses was summed for m/z 50−450, plus the fragment at m/z 91, which represents a significant fragment ion for toluene. This range excludes light gases from the analysis but includes most of the significant signals from the condensable organic molecules. Using only the even-numbered molecular weights excludes small peaks from fragment ions from the MBMS. Parenthetically, a rough calibration scheme for total tars has been developed using the MBMS, was shown to produce accurate results at high temperatures,[33] but was less accurate at lower temperatures. Because our study was focused on a wide temperature range, we elected not to use this calibration scheme and are instead focusing on a comparison of the integrated intensities for different tar species and the total tar signal.

Table 2. Elemental and Proximate Analyses of White Oak[a]

loss on drying (wt %)	5.28
elemental analysis (wt %, dry and ash free)	
C	50.1
O	43.3
H	5.5
N	0.3
S	0.2
proximate analysis (wt %, dry)	
volatile matter	85.9
fixed carbon	13.6
ash	0.5
high heating value (BTU/lb dry biomass)	8313

[a] Measured by Hazen Research, Inc. according to referenced American Society for Testing and Materials (ASTM) standards.[34]

A $^1/_4$ in. stainless-steel tube directed a sample of the gas through a coldfinger, a coalescing filter, and a backpressure regulator to light gas analytical instruments: (1) a thermal conductivity detector (TCD, Nova model 430) and (2) a four-channel, NDIR (Fuji model ZRE). These analyzed the cooled gas for H_2, CO, CO_2, and O_2. The NDIR and TCD were calibrated twice over the course of the experiments using National Institute of Standards and Technology (NIST)-traceable standard gases and house nitrogen. Initially, a more intensive calibration of the TCD measured the response to three light gases present in syngas, which were measured by the NDIR (CO, CO_2, and CH_4). The TCD response to these gases was subtracted out of the total response, and the response of hydrogen was obtained. Methane

caused a linear response in the TCD signal; CO and CO_2 invoked no response.

Experiments. Four particle sizes (6, 13, 18, and 25 mm) were fed to the 4FBR at five temperatures (500, 600, 700, 800, and 900 °C) using a full-factorial design with three replicates at each particle size/temperature combination. The average gas residence time was kept constant at each temperature as was the bed inventory. The sample weight was kept approximately constant at an average of 8.3 ± 0.4 g. A total of 1 sphere was fed for the 25 mm particles, while 3 were used for the 18 mm particles, 8 for the 13 mm particles, and 80 for the 6 mm particles. All samples were milled from one white oak board; analysis of white oak is given in Table 2.

A spherical geometry was chosen for the particles in this study to allow us to compare experimental and modeling results with previous work.[13,25] We chose this range of sphere sizes to observe heat- and mass-transfer effects through the particle while working within the geometry limitations of the reactor and feed system. Smaller particles would have been difficult to feed consistently with this feed configuration. Because our particles were spherical, the effect of particle geometry and aspect ratio on product yields was outside the scope of these experiments.

For these experiments, the main fluidizing gas was nitrogen, with a small amount of argon (UHP) as an inert tracer gas; these flowed through the coiled preheater and then entered the main body of the reactor through the distribution plate. Biomass particles were fed batchwise into the top third of the fluidized bed via the feed tube, were heated by the fluidized olivine bed, and thus, gasified. After each batch experiment, the fluidizing nitrogen was replaced with an equal mass flow of air to combust the char. The amount of char remaining in the reactor after pyrolysis was calculated from the total moles of carbon, as measured from the evolved CO_2 and CO during the burnoff step. The burnoff step kept the bed inventory constant as well, because no char remained in the reactor; any remaining ash would have been entrained in the exhaust and filtered out in the cold gas stream. Finally, the reactor was purged with nitrogen gas until the oxygen concentration returned to zero before the next biomass sample was fed. On two occasions, we gasified particles and then cooled the reactor under nitrogen to collect the char samples.

In these experiments, fluidization gas flows between 22 and 33 sL min^{-1} were used to maintain an average reactor residence time of about 2.5 s and an average gas velocity of about 19 cm s^{-1}. These linear gas velocities were between 3.5 and 4.7 times the calculated minimum fluidization velocity of olivine for each temperature. Pressure was kept relatively constant at 6 kPa; however, the pressure increased upon feeding biomass.

Olivine (magnesium iron silicate, AGSCO Corp.) was used as the fluidizing medium with a weight-average particle size of 270 μm. Olivine was loaded to the height of the bottom of the feed tube (20 cm, unfluidized, approximately 3 kg). Olivine was chosen as the bed material over the more common silica sand because the latter can form low-melting-point silicates with alkali salts from biomass ash, which can lead to bed agglomeration at gasification temperatures and especially during burnouts.[35]

Statistical Analyses. To more effectively analyze the mass spectra from this study, multivariate analysis was used to find trends in the data. Because each mass spectrum contained hundreds of peaks and there were over 50 experiments, finding trends in the data solely based on observation using the raw data would have been problematic. Multivariate analysis is a statistical tool that is used to analyze the data to identify pure components (PCs) of masses that are correlated. The multivariate curve resolution (MCR) optimized by alternating least squares routine available in the statistical analysis software package, The Unscrambler (Camo Software, AS, version 9.7), was used for this analysis. This approach yields loadings for each PC as a function of experimental conditions, which are related to the concentration of that
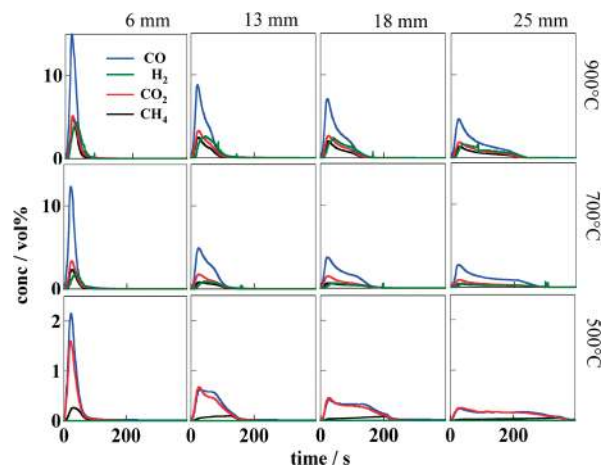

Figure 2. Formation of light gases from the gasification of different particle sizes of white oak.

group of compounds. The score plots for each PC are effectively mass spectra showing the composition of that PC. These plots are often useful for identifying product trends in biomass pyrolysis data and can be used to extract kinetic parameters.[11,27,32,36−38]

Light gas results were analyzed using R 2.13.0 (R Development Core Team[39]). A one-way analysis of variance (ANOVA) was conducted for each temperature and each particle size. A pairwise t test with a Bonferroni correction identified significant differences between each temperature at a constant particle size and vice versa to 95% confidence interval. Essentially identical results were achieved using the Tukey honest significant difference (HSD) test. These detailed results are included as Supporting Information.

■ RESULTS AND DISCUSSION

As outlined in the Experimental Section, four wood sphere sizes were gasified at five temperatures in the 4FBR. The feeding system functioned adequately, but the sliding interface between the plunger rod and the feed tube allowed a small amount of vapor to escape before the feeding system could be resealed. This leak was more problematic for the smallest particle sizes and the highest temperatures because gasification rates were fastest for these conditions; as a result, standard deviation error bars tend to be larger for these conditions, and the light gas yield data may have been slightly underestimated. During gasification, the bed temperature fluctuated less than 1% of the set point and the reactor pressure was observed to increase about 2-fold at the peak of gas evolution.

Light Gas and Char Production. Evolution of light gases from the wood spheres showed an indication of heat- and mass-transfer restrictions. Figure 2 shows the evolution of the measured gas pulses during typical experiments for all four particle sizes at 500, 700, and 900 °C. As can be seen, the widths of the peaks at each temperature increase with increasing particle diameter. For all particle sizes, the gas evolution maintained a relatively sharp feature at the beginning of the evolution with a lower intensity tail extending to longer times for the larger spheres. Similar gas release profiles were observed by Jand and Foscolo[25] and Rapagnà and di Celso[13] for similar experiments with spherical wood particles. When the biomass particle enters the reactor, its surface temperature quickly increases because of a high rate of heat transfer from the hot bed materials and the devolatilization process begins almost immediately. In contrast,
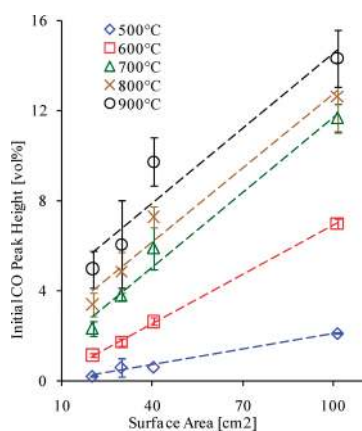
Figure 3. Initial peak height of the gas pulse as a function of the total surface area of particles in the reactor.
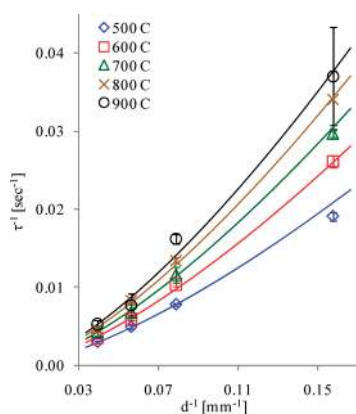

Figure 4. Evolution of the inverse of the devolatilization time as a function of the inverse of the initial diameter for temperatures between 500 and 900 °C and diameters between 6 and 25 mm. Comparison between experimental data (symbols) and power law fit from eq 2 (lines).
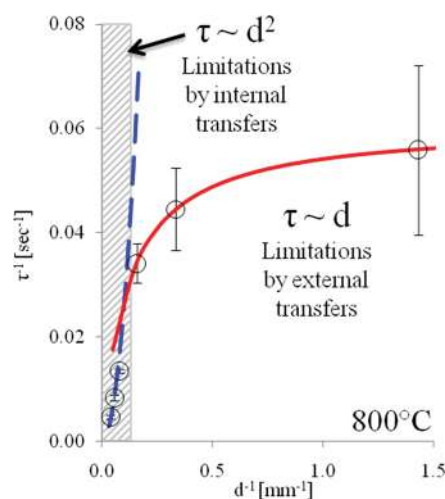

Figure 5. Evolution of the inverse of the devolatilization time as a function of the inverse of the initial diameter at 800 °C for a wider range of particle sizes, showing the transition between internal and external heat- and mass-transport limitations.

Figure 4 shows the inverse of the devolatilization time, τ, defined as the total duration of the recorded pulse, as a function of the inverse of particle diameter. τ increases with the particle size, which indicates that the process is limited by mass and heat transfer to and from the particle rather than by the chemistry. In this regime, a commonly used model to describe the total devolatilization time, τ, as a function of the initial particle size, d_0, is a simple power law

$$\tau = Ad_0^{n} \tag{1}$$

where A and n are fitted to match the experimental data. In the present case, it was found that n is independent of the temperature, while the prefactor A depends exponentially upon the temperature, leading to the following expression:

$$\tau = e^{1013.2/T^{1.076}} d_0^{1.414} \tag{2}$$

The value $n = 1.414$ is well within the range of values reported previously for both biomass and coal devolatilization.[13,16] As shown in Figure 4, this model is able to accurately reproduce the experimental devolatilization time.[25]

As the particle diameter goes to zero, the devolatilization time predicted by the power law model also goes to zero, thereby wrongly indicating infinitely fast kinetics. To appreciate the range of validity of the power law model, we conducted two additional particle size experiments at 800 °C with sieved particles from ground white oak pellets averaging 3 and 0.7 mm. These additional data are displayed in Figure 5, along with the larger spheres data, showing a significant change of behavior as the particle size decreases. To explain this change of slope, a time scale analysis following the work by Dupont et al.[40] was conducted. It shows that, for the largest particle sizes (i.e., above about 10 mm), the devolatilization time is proportional to the square of the particle diameter (dashed blue line in Figure 5), indicating internal heat- and mass-transfer limitations. Below that, a much better fit is obtained using a linear dependence upon the particle diameter (solid red line in Figure 5), which is consistent with external transfer limitations.[40] This analysis also explains the power law exponent between 1 and 2 found in eq 1, because this expression was derived from particle size data
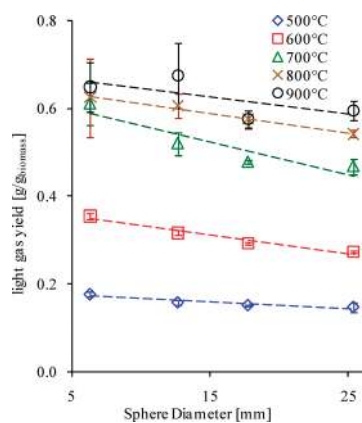
the inner regions of the biomass particles are slower to heat up to the bed temperature, in part because of the low thermal diffusivity of biomass. In addition, the porosity of the biomass restricts the flow of the gases, further delaying the release of the volatiles and resulting in the long tails in the observed profiles for larger spheres. Some evidence of particle fragmentation was observed in the char particles removed from the bed after the reactor had been cooled, especially for the largest particles. We do not believe that fragmentation affected the results shown in Figure 2 and probably took place after devolatilization. If fracturing were a factor, the size of the larger particles would be effectively reduced and we would expect the shapes of the curves for the smallest and largest particle sizes to be more similar.

The initial pulse of gas comes from devolatilization of the outer layers of the biomass and, thus, should correlate with the surface areas of the spheres. A comparison of the total surface areas for each batch and the initial pulse height intensities are shown in Figure 3. Error bars in this and all figures represent the standard deviation of the three replicates. As can be seen, the peak heights are roughly proportional to the surface area. That is, the peak height is linearly dependent upon the surface area, with coefficient of determination (R^2) values for the linear regression between 0.92 and 1.00 for all five temperatures.

Figure 6. Sum of light gas yields (CO, CO_2, CH_4, and H_2) on a dry basis plotted as a function of the diameter of the white oak spheres pyrolyzed.

Figure 7. Char yield on a dry basis as a function of the sphere diameter.

covering both regimes. Data from particles smaller than 0.7 mm would be necessary to illustrate the transition to kinetic control, for which the devolatilization time is independent from the particle diameter.

A comparison can be made of the yields of CO, CO_2, CH_4, and H_2, the total yield of light gas, and the char yield. An overall mass balance was not calculated for these results, because water, tar, and some light gases were not directly measured. The yields are determined by integrating the peaks, such as those shown in Figure 2, converting the values to mass, and dividing by the dry mass of biomass feed; because the ash content of the particles was constant for all experiments, we did not correct the mass of the feed on an ash-free basis. The total light gas yield was determined by summing the yields for CO, CO_2, CH_4, and H_2 (species with two or more carbon atoms were not included because their concentrations were not directly measured nor was water). The averages of these sums are plotted as a function of the particle size and temperature in Figure 6. From the pairwise t-test analyses (included in the Supporting Information), we can conclude that the light gas yield increases with increasing temperature and then starts to plateau at higher temperatures. The plateau starts earlier for smaller particles (700 °C for 6 mm), and the largest particle size does not plateau at all (all temperatures are significant). The results of the t tests correspond to the trends of the data and the error bars in Figure 6.

At 500 °C, most of the volatile material in the biomass vaporized from the particles but evolved mostly as condensable organic vapors with only a small yield of light gases. As the temperature increased, these pyrolysis products cracked and more light gases were formed. At 800 and 900 °C, diminishing returns are seen when increasing the reaction temperature, in an attempt to increase light gas yield. These results are consistent with those by Carpenter et al.,[28] who found that total light gas yield increased with increasing temperature until reaching a plateau at 750−870 °C for particles smaller than ours.

The total gas production appears to decrease with increasing sphere size, although the statistical analysis shows that we can only draw this conclusion for 600 °C and the smallest versus two largest sizes for 500 and 700 °C; no differences were found between particle sizes for 800 or 900 °C. The gas production decrease is likely due to heat- and/or mass-transfer limitations within the particle. There is also a diminishing rate of change in light gas yield with increasing particle size. Rapagnà and di
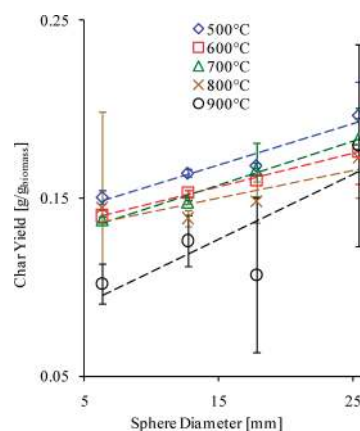
Celso[13] found the same behavior in their study at similar temperatures and particle sizes. With larger spheres, the wood and subsequent char act more effectively to insulate the inner part of the particles, and the slower heating rate at the center of the larger sphere prevents the particle from being pyrolyzed uniformly; the same slow heating rate creates conditions that trap the gases and tars in the larger spheres and allows them to react to form char,[11,15,41,42] a hypothesis that is supported by the data shown in Figure 7 and discussed below. At higher temperatures, heat- and mass-transfer rates are increased, particles heat faster, and less tars and char are formed. As a result, particle size has less influence on the light gas evolution at higher reactor temperatures.

Figure 7 shows the char yield as a function of particle size and temperature and represents the calculated amount of char remaining in the reactor after all gasification products had volatilized. The graph indicates that char production increases with an increasing particle size and decreases with increasing temperature. The pairwise t test supports this to a degree but only indicates significant differences between the 6 and 25 mm particles at 500, 600, and 700 °C, with no difference indicated for particle size at 800 and 900 °C; this is likely attributable to the large scatter in the data at those temperatures and the low number of degrees of freedom based on the number of replicates. With regard to temperature, the 13 mm particles showed a significant dependence upon temperature between the three lowest and the highest temperature (all other particle sizes contained too much scatter in the data to show differences). Because the mass of char remaining in the reactor is calculated from several measured values, any error in these values is compounded several times, which accounts for the large amount of scatter in the data set. Those char trend results, which are statistically significant, are consistent with observations by Rapagnà and di Celso.[13]

The statistically significant char data do indicate that faster heating rates produce less char. For larger particles and lower temperatures, carbon tends to form more char, and this ultimately lowers light gas yield. Figures 6 and 7 are consistent in this way, in that larger particles produce fewer light gases and more char. These results for char and light gas production agree with the observations of others,[13,14,25] as well as the well-known differences between slow pyrolysis to make charcoal versus fast pyrolysis to make oils.
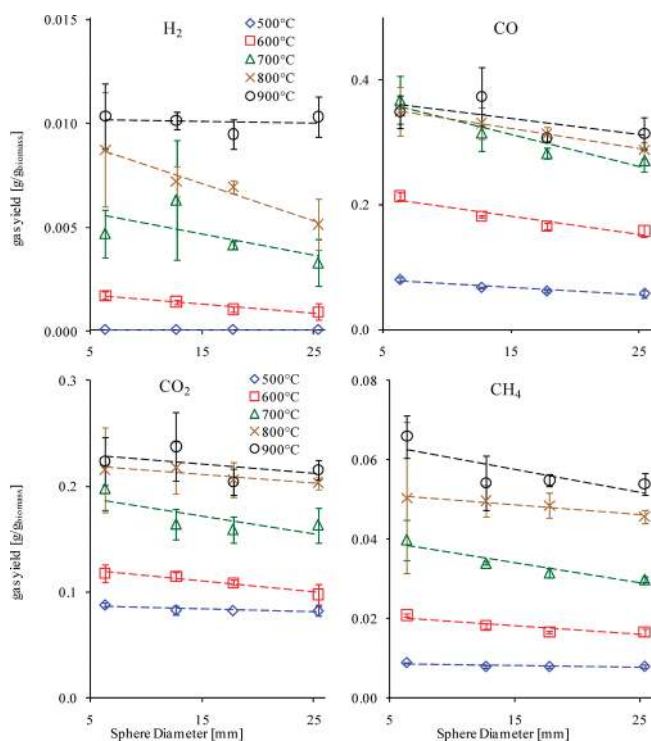
Figure 8. H_2, CO, CO_2, and CH_4 gas yields on a dry basis as a function of the particle size and temperature.

Figure 9. Typical MBMS spectra from gasification of 6 mm white oak spheres in the 4FBR at (a) 900 °C, (b) 700 °C, and (c) 500 °C.

The yields of the four measured light gases as a function of sphere size are plotted in Figure 8. Similar trends, which are also consistent with those for the total yield in Figure 6, are seen for each species. As expected, more of each species is produced with increasing temperature in all cases. All individual gas yields gently decrease with increasing sphere size or remain constant as in the lowest temperature cases, and all light gas yields increase with increasing temperature, with this being most pronounced for CO based on the scale on the *y* axis. These results agree moderately with those by Jand and Foscolo,[25] who concluded that CO production was the light gas influenced most by sphere diameter.

MBMS Data. The MBMS spectra of the hot gas from the 4FBR provide information about the relative concentrations as well as the molecular species of the tars. As was demonstrated in earlier studies,[11,30,32] the total amount of tars generally decreases with increasing pyrolysis temperature because of thermal cracking of the primary pyrolysis products. However, the more refractory PAHs tend to increase with increasing temperatures. Figure 9 plots typical raw mass spectra obtained by averaging the signal over the pulse of gas and subtracting a background spectrum obtained when only inert gas was flowing through the reactor. The figure shows spectra obtained using the 6 mm spheres with reactor temperatures of 500, 700, and 900 °C. The mass spectra are typical for what has been observed in past MBMS studies of biomass pyrolysis.[11,27] A comparison of the mass spectra for different particle sizes showed the same relative intensity for the individual peaks, indicating that the tar species present in the vapor phase did not change with sphere size, although the absolute intensity of the peaks does change.

At 500 °C (Figure 9c), the ions observed result from the vaporization of the biopolymers in the oak. For instance, the peaks at m/z 180 and 154 arise from lignin, while m/z 124, 110, 96, 60, and 43 arise from carbohydrates. The products seen at
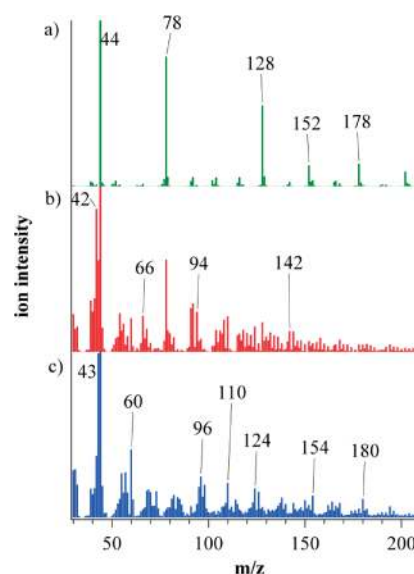
700 °C in Figure 9b are a result of significant cracking of the primary vapors. For instance, the peak m/z 142 is due to methyl naphthalene; the peak at m/z 94 is due to phenol; the peak at m/z 66 is due to cyclopentadiene; and the peak at m/z 42 is due to propylene. These products are not directly volatilized from biomass but result from the thermal cracking of pyrolysis vapors from lignin and carbohydrates. At 900 °C (Figure 9a), the tars have been converted into PAHs, such as m/z 178 (phenanthrene and anthracene), m/z 152 (flourene), m/z 128 (naphthalene), and m/z 78 (benzene). These PAHs are formed at high temperatures by molecular-weight growth reactions involving small molecules and radicals that are produced from cracking reactions.[11] The molecular-weight growth reactions leading to PAHs have been extensively studied because of their relevance in combustion applications,[43] and detailed kinetic mechanisms describing this process are now available.[44] Note that m/z 44, CO_2, is also a significant peak in this and the other spectra. Methane, m/z 16, was also observed in the mass spectra but is not shown here. The peak for CO, m/z 28, could not be observed because of interference with N_2, also m/z 28 and the carrier gas, whose concentration would have saturated the detector. The peak for H_2, m/z 2, was not measured because of the settings of the mass spectrometer. However, these light gases were measured with NDIR and TCD, as discussed above.

The MBMS spectra were used to estimate the relative quantities and types of tars formed during the pyrolysis experiments and to identify trends with sphere size. Figure 10 shows the measured signal for the total tars as a function of the sphere size and temperature. The total tar trends with particle size and temperature are consistent with the light gases in Figure 6 and char yields in Figure 7. As can be seen, the tars decrease with increasing temperature. This result is consistent with previous experimental observations.[11,28] The increase in the temperature leads to cracking of the tar molecules to form more light gases. At the higher temperatures (>700 °C), small molecules and radicals combine to form PAHs, leading to an increase in tertiary tars with increasing temperature, as discussed below. This explains why the tar signal does not significantly decrease
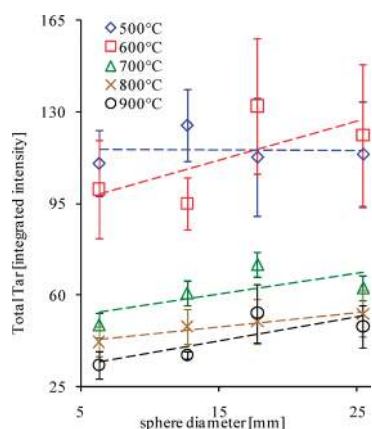
Figure 10. Measured tar signals (sum of even peaks from m/z 50 to 450) as a function of the sphere size and temperature.

Figure 11. Evolution of PAH formation (the sum of m/z 78, 102, 104, 116, 128, 152, 178, and 202) with sphere size and temperature.

above 700 °C. The tar signal at all temperatures shows an overall increase with increasing sphere size, supporting the hypothesis that larger particles produce more tar and char and lower light gas yields. However, the statistical analysis of the total tar comparison with respect to sphere diameter does not indicate significant differences for the temperatures in this study. This is attributable to the large scatter in the data indicated in Figure 10 by the large error bars. We expect that this conclusion is valid, but the MBMS is not sensitive enough to detect and quantify the slight increases observed. When the total tar yield is calculated by difference from the measured light gas products, the same trends are observed but the pairwise t test does indicate differences between the smallest and largest particle sizes for the three lowest temperatures. This calculation is an estimation of total tar, because it also includes water and the light gases not measured.

We have particular interest in trends and quantities of PAHs because these are the most refractory tars and are generally formed with increasing temperature. The total signal for the PAHs was determined by adding the signals for the most prominent aromatic species found at 900 °C (shown in Figure 9a): m/z 78 (benzene), m/z 102 (phenyl acetylene), m/z 104 (styrene), m/z 116 (indene), m/z 128 (naphthalene), m/z 152 (fluorene), m/z 178 (anthracene and phenanthrene), and m/z 202 (pyrene). A plot of the sum of the signals for these species as a function of the sphere size and temperature is shown in Figure 11. As can be seen in the figure, the PAHs show a strong dependence upon the temperature, with a marked increase between 700 and 800 °C, which is consistent with tar/tempera-ture data observed in previous experiments.[11] PAHs also increase with increasing sphere size. Similar to the total tars, the large error bars and the pairwise t test in the statistical analysis of the PAH signals do not indicate significant differences based on particle size, although the Tukey HSD indicates significance between the smallest and two largest particle sizes.

Multivariate Analysis of MBMS Data. The MCR method of multivariate analysis was conducted to analyze overall trends in the MBMS data set, which included triplicates at five tempera-tures, 500, 600, 700, 800, and 900 °C, and four particle sizes, 6, 13, 18, and 25 mm. Mass spectra using ion signals from 200 masses with the greatest variance in the set were included in this analysis. Three PCs best described the variance in the data. The loadings for each PC are presented in Figure 12, which are
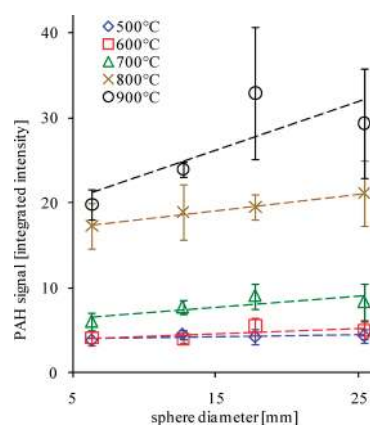
essentially the mass spectra of each PC. The scores, which are related to the concentrations, are plotted versus temperature in Figure 13. These plots are consistent with earlier studies.[11,27,29,32]
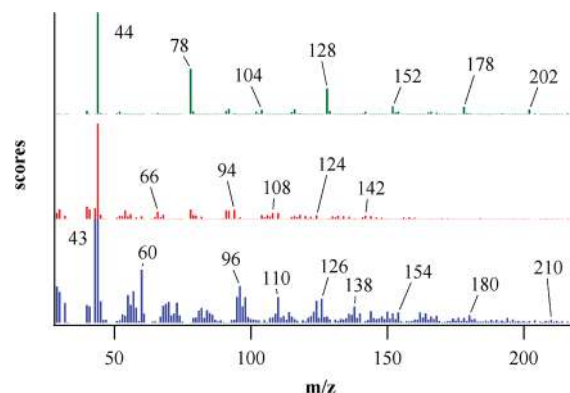

Figure 12. Component scores obtained from MCR analysis of the MBMS data of the pyrolysis of oak spheres in the 4FBR. From top to bottom, PC3 is green, PC2 is red, and PC1 is blue. The scores correspond to the relative molar concentration of each m/z ratio.

Evans and Milne studied the pyrolysis of small samples (50 mg) of biomass in hot helium and analyzed the MBMS data using the multivariate software package called ISMA.[27] They described their data with three factors, which they termed primary, secondary, and tertiary pyrolysis products. Jablonski et al. showed that the ISMA technique produced the same results as MCR for an MBMS data set obtained from pilot gasification experiments.[32] Jarvis et al. analyzed the tars formed from the pyrolysis of ground oak pyrolyzed in an entrained flow reactor.[11] In that study, six PCs were identified with MCR. More PCs were obtained from that data set because measurements were made in 25 °C increments. We were only able to extract three PCs because of the comparatively large temperature increment (100 °C). The six PCs found by Jarvis et al. can be compressed into the three factors observed here.

The three PCs shown in Figure 12 are similar to those found in the study by Evans and Milne and Jablonski et al. PC1 is composed of primary pyrolysis products. PC2 is composed of products that result from the cracking of the primary products. PC3 is aromatic hydrocarbons or PAHs. For instance, PC1 contains peaks from lignin products at m/z 138, 154, 180, and
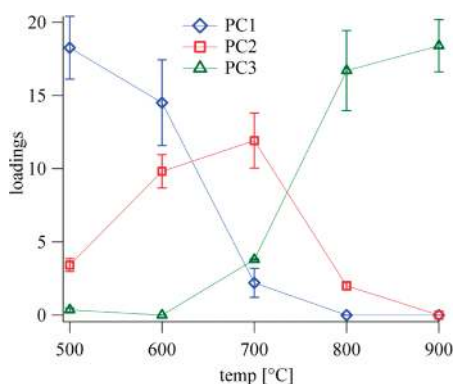
Figure 13. Changes in the loadings of PC1 (blue), PC2 (red), and PC3 (green) shown in Figure 12 as a function of the reactor temperature. PC1 represents primary pyrolysis vapor. PC2 represents secondary products. PC3 represents PAHs. The loadings are related to the concentrations of the components for each PC given in the scores plot. These results are for 6 mm spheres, but similar trends were observed for the other sphere sizes.

210 from methylguaiacol, coumaryl alcohol, coniferyl alcohol, and sinapyl alcohol and peaks from carbohydrates, such as m/z 43, 60, 96, 110, and 126 from acetyl fragment, acetic acid, furfural, 5-methylfurfural, and 5-hydroxymethylfurfural. The PC2 peaks shown are from cyclopentadiene (m/z 66), phenol (m/z 94), cresol (m/z 108), guaiacol (m/z 124), and methylnaphthalene (m/z 142). The peaks in the PC3 spectrum are the PAHs identified above. The temperature profiles shown in Figure 13 are consistent with the assignment of the PCs discussed above. The primary vapors evolve at 500 °C and decrease with increasing temperature. The cracking products increase with temperature from 500 °C and reach a maximum between 600 and 700 °C. The PAHs increase with temperature starting at 600 °C.

A plot of the loadings of the PCs as a function of the particle size is presented in Figure 14. In this plot, the PCs are presented at the temperature where they reach their maximum in Figure 13, namely, 500 °C for PC1, 700 °C for PC2, and 900 °C for PC3. As can be seen, PC1 only changes by a small amount (10%) when changing the sphere diameter, whereas PC2 and PC3 increase by roughly a factor of 2 when the particle size increases from 6 to 25 mm diameter, although the larger error bars for the larger particle sizes indicate that these increases could be less pronounced than the averages indicate. Results in Figure 14 combined with Figure 2 indicate that the secondary reactions, which form PAHs, are more prevalent in larger particles and, therefore, are likely forming inside the particle. The gas concentrations as a function of time for the 25 mm particles in Figure 2 are much lower outside the particle than for the smaller particles as a result of the slow devolatlization time. We can conclude that PAH formation must be occurring inside the particle to form higher concentrations for the larger particles, because bimolecular reactions outside the particle would have slower reaction rates based on the concentration.

■ CONCLUSION

Gas evolution profiles for oak sphere sizes up to 25 mm at different temperatures indicated strong heat- and mass-transfer effects within the particle. A power law model captured the devolatilization time of the four largest solid particle sizes but failed to correctly predict this for smaller sizes, indicating a
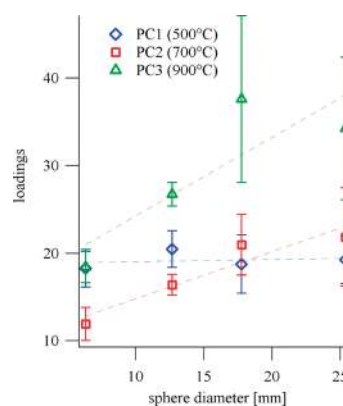

Figure 14. Intensities (loadings) of PC1 at 500 °C (blue), PC2 (red) at 700 °C, and PC3 (green) at 900 °C as a function of the sphere diameter. PC1 represents primary pyrolysis vapor. PC2 represents secondary products. PC3 represents PAHs. The intensities are given at the maximum temperature for each PC.

change of regime from internal to external heat- and mass-transfer limitations. Even for the smallest sizes investigated, the chemical kinetics were not found to be the controlling process.

The light gas, tar, and char yields were in accordance with the heat- and mass-transfer-limited behavior and showed that slower heating rates in the interior of the larger particles led to more tar and char formation and, therefore, less efficient gasification. We also found that PAHs increased with increasing particle size as a result of secondary reactions occurring inside the particles. We draw these conclusions cautiously based on the statistical analyses for the char, total tar, and PAHs for the particle sizes in this study. These findings could potentially have implications for the overall economics for commercial-scale indirectly heated, dual-fluidized-bed biomass gasification processes, because the feedstock preparation cost (the amount of milling required) could be balanced with gasification efficiency in terms of light gas versus char production, as well as the amount of tar that must be reformed or otherwise managed downstream of the gasifier. These implications of the heat- and mass-transfer limitations that were present in our study could potentially be mitigated by limiting the dimension of particles along one axis, while taking advantage of the natural tendency of the feedstock to cleave in one direction, such as with wood chips. A technoeconomic analysis of the process, which was outside the scope of this paper, would show if a cost benefit of additional feedstock preparation exists.

■ ASSOCIATED CONTENT

ⓢ Supporting Information. Statistical analyses for individual light gas yields, total light gas yield, char yield, total tar, total tar by difference, and PAHs; also additional plots of the sum of light gas, char, and calculated ash yields and tar yield by difference, a histogram of the mass balance for the average at each set of conditions, and a histogram showing average dry and nitrogen-free gas compositions. This material is available free of charge via the Internet at http://pubs.acs.org.

■ AUTHOR INFORMATION

Corresponding Author

*E-mail: katherine.gaston@nrel.gov.

■ REFERENCES

(1) Kinoshita, C.; Wang, Y.; Zhou, J. Tar formation under different biomass gasification conditions. *J. Anal. Appl. Pyrolysis* **1994**, *29* (2), 169–181.

(2) Kiel, J. H. A.; van Paasen, S. V. B.; Neeft, J. P. A.; Devi, L.; Ptasinski, K. J.; Janssen, F. J. J. G.; Meijer, R.; Berends, R. H.; Temmink, H. M. G.; Brem, G.; Padban, N.; Bramer, E. A. Primary measures to reduce tar formation in fluidized-bed biomass gasifiers. *Final Report SDE Project P1999-012*; Dutch Agency for Research in Sustainable Energy (SDE): The Hague, The Netherlands, 2004; Report ECN-C-04-014, pp 1–108.

(3) Corella, J.; Caballero, M.; Aznar, M.; Brage, C. Two advanced models for the kinetics of the variation of the tar composition in its catalytic elimination in biomass gasification. *Ind. Eng. Chem. Res.* **2003**, *42* (13), 3001–3011.

(4) Phillips, S. D. Technoeconomic analysis of a lignocellulosic biomass indirect gasification process to make ethanol via mixed alcohols synthesis. *Ind. Eng. Chem. Res.* **2007**, *46* (26), 8887–8897.

(5) Devi, L.; Ptasinski, K. J.; Janssen, F. J. J. G. A review of the primary measures for tar elimination in biomass gasification processes. *Biomass Bioenergy* **2003**, *24* (2), 125–140.

(6) Narvaez, I.; Orio, A.; Aznar, M.; Corella, J. Biomass gasification with air in an atmospheric bubbling fluidized bed. Effect of six operational variables on the quality of the produced raw gas. *Ind. Eng. Chem. Res.* **1996**, 35 (7), 2110–2120.

(7) Corella, J.; Aznar, M.; Delgado, J.; Aldea, E. Steam gasification of cellulosic wastes in a fluidized-bed with downstream vessels. *Ind. Eng. Chem. Res.* **1991**, *30* (10), 2252–2262.

(8) Corella, J.; Herguido, J.; Alday, F. J. Pyrolysis and steam gasification of biomass in fluidized beds. Influence of the type and location of the biomass feeding point on the product distribution. In *Research in Thermochemical Biomass Conversion*; Bridgwater, A. V., Kuester, J. L., Eds.; Elsevier Applied Science: London, U.K., 1988; pp 384–398.

(9) Gil, J.; Aznar, M.; Caballero, M.; Frances, E.; Corella, J. Biomass gasification in fluidized bed at pilot scale with steam–oxygen mixtures. Product distribution for very different operating conditions. *Energy Fuels* **1997**, *11* (6), 1109–1118.

(10) Gil, J.; Corella, J.; Aznar, M.; Caballero, M. Biomass gasification in atmospheric and bubbling fluidized bed: Effect of the type of gasifying agent on the product distribution. *Biomass Bioenergy* **1999**, *17* (5), 389–403.

(11) Jarvis, M. W.; Haas, T. J.; Donohoe, B. S.; Daily, J. W.; Gaston, K. R.; Frederick, W. J.; Nimlos, M. R. Elucidation of biomass pyrolysis products using a laminar entrained flow reactor and char particle imaging. *Energy Fuels* **2011**, *25* (1), 324–336.

(12) Yu, Q.; Brage, C.; Chen, G.; Sjöström, K. Temperature impact on the formation of tar from biomass pyrolysis in a free-fall reactor. *J. Anal. Appl. Pyrolysis* **1997**, *40–41*, 481–489.

(13) Rapagnà, S.; di Celso, G. M. Devolatilization of wood particles in a hot fluidized bed: Product yields and conversion rates. *Biomass Bioenergy* **2008**, *32* (12), 1123–1129.

(14) Herguido, J.; Corella, J.; Gonzalez-Saiz, J. Steam gasification of lignocellulosic residues in a fluidized bed at a small pilot scale. Effect of the type of feedstock. *Ind. Eng. Chem. Res.* **1992**, *31* (5), 1274–1282.

(15) Haas, T. J.; Nimlos, M. R.; Donohoe, B. S. Real-time and post-reaction microscopic structural analysis of biomass undergoing pyrolysis. *Energy Fuels* **2009**, *23* (7), 3810–3817.

(16) de Diego, L.; Garcia-Labiano, F.; Abad, A.; Gayan, P.; Adanez, J. Modeling of the devolatilization of nonspherical wet pine wood particles in fluidized beds. *Ind. Eng. Chem. Res.* **2002**, *41* (15), 3642–3650.

(17) Di Blasi, C.; Branca, C. Temperatures of wood particles in a hot sand bed fluidized by nitrogen. *Energy Fuels* **2003**, *17* (1), 247–254.

(18) Ross, D. P.; Heidenreich, C. A.; Zhang, D. K. Devolatilisation times of coal particles in a fluidised-bed. *Fuel* **2000**, *79* (8), 873–883.

(19) Di Blasi, C. Modeling chemical and physical processes of wood and biomass pyrolysis. *Prog. Energy Combust. Sci.* **2008**, *34* (1), 47–90.

(20) Lu, H.; Ip, E.; Scott, J.; Foster, P.; Vickers, M.; Baxter, L. L. Effects of particle shape and size on devolatilization of biomass particle. *Fuel* **2010**, *89* (5), 1156–1168.

(21) Di Blasi, C. Physico-chemical processes occurring inside a degrading two-dimensional anisotropic porous medium. *Int. J. Heat Mass Transfer* **1998**, *41* (24), 4139–4150.

(22) Bharadwaj, A.; Baxter, L.; Robinson, A. Effects of intraparticle heat and mass transfer on biomass devolatilization: Experimental results and model predictions. *Energy Fuels* **2004**, *18* (4), 1021–1031.

(23) Miller, R. S.; Bellan, J. Analysis of reaction products and conversion time in the pyrolysis of cellulose and wood particles. *Combust. Sci. Technol.* **1996**, *119*, 331–373.

(24) Miller, R. S.; Bellan, J. A generalized biomass pyrolysis model based on superimposed cellulose, hemicellulose and lignin kinetics. *Combust. Sci. Technol.* **1997**, *126* (1), 97–137.

(25) Jand, N.; Foscolo, P. U. Decomposition of wood particles in fluidized beds. *Ind. Eng. Chem. Res.* **2005**, *44* (14), 5079–5089.

(26) Hernández, J. J.; Aranda-Almansa, G.; Bula, A. Gasification of biomass wastes in an entrained flow gasifier: Effect of the particle size and the residence time. *Fuel Process. Technol.* **2010**, *91* (6), 681–692.

(27) Evans, R. J.; Milne, T. A. Molecular characterization of the pyrolysis of biomass. 1. Fundamentals. *Energy Fuels* **1987**, *1* (2), 123–137.

(28) Carpenter, D. L.; Bain, R. L.; Davis, R. E.; Dutta, A.; Feik, C. J.; Gaston, K. R.; Jablonski, W.; Phillips, S. D.; Nimlos, M. R. Pilot-scale gasification of corn stover, switchgrass, wheat straw, and wood: 1. Parametric study and comparison with literature. *Ind. Eng. Chem. Res.* **2010**, *49* (4), 1859–1871.

(29) Evans, R. J.; Milne, T. A.; Soltys, M. N. Direct mass-spectrometric studies of the pyrolysis of carbonaceous fuels. 3. Primary pyrolysis of lignin. *J. Anal. Appl. Pyrolysis* **1986**, *9* (3), 207–236.

(30) Evans, R. J.; Milne, T. A. Molecular characterization of the pyrolysis of biomass. 2. Applications. *Energy Fuels* **1987**, *1* (4), 311–319.

(31) Agblevor, F. A.; Evans, R. J.; Johnson, K. D. Molecular-beam mass-spectrometric analysis of lignocellulosic materials. 1. Herbaceous biomass. *J. Anal. Appl. Pyrolysis* **1994**, *30* (2), 125–144.

(32) Jablonski, W.; Gaston, K. R.; Nimlos, M. R.; Carpenter, D. L.; Feik, C. J.; Phillips, S. D. Pilot-scale gasification of corn stover, switchgrass, wheat straw, and wood: 2. Identification of global chemistry using multivariate curve resolution techniques. *Ind. Eng. Chem. Res.* **2009**, *48* (23), 10691–10701.

(33) Carpenter, D. L.; Deutch, S. P.; French, R. J. Quantitative measurement of biomass gasifier tars using a molecular-beam mass spectrometer: Comparison with traditional impinger sampling. *Energy Fuels* **2007**, *21* (5), 3036–3043.

(34) American Society for Testing and Materials (ASTM). *ASTM Standard D2013, Preparing Coal Samples for Analysis*; *ASTM Standard D3172, Proximate Analysis of Coal and Coke*; *ASTM Standard D3176, Ultimate Analysis of Coal and Coke*; *ASTM Standard D3173, Moisture in the Analysis Sample of Coal and Coke*; *ASTM Standard D3174, Ash in the Analysis Sample of Coal and Coke*; *ASTM Standard D3175, Volatile Matter in the Analysis Sample of Coal and Coke*; *ASTM Standard D4239, Sulfur in the Analysis Sample of Coal and Coke (High Temp Methods)*; *ASTM Standard D5373, Instrumental Determination of Carbon, Hydrogen,*

and Nitrogen; and *ASTM Standard D5865, Gross Calorific Value of Coal and Coke*; ASTM: West Conshohocken, PA, in various years.

(35) Bartels, M.; Lin, W.; Nijenhuis, J.; Kapteijn, F.; van Ommen, J. R. Agglomeration in fluidized beds at high temperatures: Mechanisms, detection and prevention. *Prog. Energy Combust. Sci.* **2008**, *34* (5), 633–666.

(36) Shin, E. J.; Nimlos, M. R.; Evans, R. J. A study of the mechanisms of vanillin pyrolysis by mass spectrometry and multivariate analysis. *Fuel* **2001**, *80* (12), 1689–1696.

(37) Shin, E. J.; Nimlos, M. R.; Evans, R. J. The formation of aromatics from the gas-phase pyrolysis of stigmasterol: Kinetics. *Fuel* **2001**, *80* (12), 1681–1687.

(38) Shin, E. J.; Nimlos, M. R.; Evans, R. J. Kinetic analysis of the gas-phase pyrolysis of carbohydrates. *Fuel* **2001**, *80* (12), 1697–1709.

(39) R Development Core Team. *R: A Language and Environment for Statistical Computing*; R Foundation for Statistical Computing: Vienna, Austria, 2011; http://www.R-project.org (accessed on May 2011).

(40) Dupont, C.; Boissonnet, G.; Seiler, J.-M.; Gauthier, P.; Schweich, D. Study about the kinetic processes of biomass steam gasification. *Fuel* **2007**, *86* (1−2), 32–40.

(41) Fushimi, C.; Araki, K.; Yamaguchi, Y.; Tsutsumi, A. Effect of heating rate on steam gasification of biomass. 2. Thermogravimetric−mass spectrometric (TG−MS) analysis of gas evolution. *Ind. Eng. Chem. Res.* **2003**, *42* (17), 3929–3936.

(42) Fushimi, C.; Araki, K.; Yamaguchi, Y.; Tsutsumi, A. Effect of heating rate on steam gasification of biomass. 1. Reactivity of char. *Ind. Eng. Chem. Res.* **2003**, *42* (17), 3922–3928.

(43) Wang, H.; Frenklach, M. A detailed kinetic modeling study of aromatics formation in laminar premixed acetylene and ethylene flames. *Combust. Flame* **1997**, *110*, 173–221.

(44) Blanquart, G.; Pepiot-Desjardins, P.; Pitsch, H. Chemical mechanism for high temperature combustion of engine relevant fuels with emphasis on soot precursors. *Combust. Flame* **2009**, *156* (3), 588–607.